

Computer-Aided Analysis of Biochanin-A as a Potential Breast Cancer Drug Based on DFT, Molecular Docking, and Pharmacokinetic Studies

Mohana Priya ¹, Azar Zochedh ², Kaliraj Chandran ², Karthick Arumugam ³, Sharmili Banu ⁴, Cibe Chakaravarthy ², Asath Bahadur Sultan ^{5,*}

¹ Department of Bioinformatics, School of Distance Education, Bharathiar University, Coimbatore, Tamil Nadu, India; mohana1308@gmail.com (M.P.);

² Department of Biotechnology, Kalsalingam Academy of Research and Education, Krishnankoil, Tamil Nadu, India; azar2411@gmail.com (A.Z.); kalirajchandran786@gmail.com (K.C.); cibe1411@gmail.com (C.C.);

³ Department of Biotechnology, Kamaraj College of Engineering and Technology, Madurai, Tamil Nadu, India; danielkarthick1@gmail.com (K.A.);

⁴ Department of Gynecology, Leonard Hospital, Batlagundu, Tamil Nadu, India; sharmilibanukr@gmail.com (S.B.);

⁵ Department of Physics, Kalsalingam Academy of Research and Education, Krishnankoil, Tamil Nadu, India

* Correspondence: s.asathbahadur@gmail.com (A.B.S.);

Scopus Author ID 57215079667

Received: 9.08.2022; Accepted: 26.08.2022; Published: 21.11.2022

Abstract: Breast cancer is the most often diagnosed and deadliest type of cancer in the world. Biochanin A is a naturally available isoflavone with various biological and pharmacological properties. In the current study, a quantum chemical investigation using density function theory (DFT) was utilized to explore the structural characteristics of biochanin A, and the breast cancer inhibitory properties were revealed through molecular docking simulation. The optimization of the lead molecule was initially performed using DFT/B3LYP approach with a 6-311++(d,p) base set. The simulated electrostatic potential was performed to evaluate the reactivity of the lead molecule, and the molecular reactivity and stability were evaluated through HOMO-LUMO analysis based on energy gap, chemical potential (μ), electronegativity (χ), hardness (η), and softness (S) values. Mulliken atomic charge distribution was performed to confirm the molecules' reactive site, and natural population analysis was performed to compute the distribution of electrons. Then molecular docking research was used to assess the interaction of biochanin A against the breast cancer target proteins, and pharmacokinetic evaluation was used to evaluate the drug-likeness property of the lead molecule. The lead molecule showed no violation against Lipinski's rule, and the highest binding affinity was observed against HER-2 (PDB ID: 2IOK) with a docking score of -9.2Kcal/mol.

Keywords: breast cancer; HOMO-LUMO; MEP; Mulliken; binding affinity; ADMET.

© 2022 by the authors. This article is an open-access article distributed under the terms and conditions of the Creative Commons Attribution (CC BY) license (<https://creativecommons.org/licenses/by/4.0/>).

1. Introduction

Generally, natural products are differentiated into various classes based on their structural similarities, such as alkaloids, saponins, terpenoids, and polyphenols [1]. Polyphenols comprise flavonoids, tannins, and lignins. Flavonoids consist of a subclass of isoflavones, phytoestrogens with a chemical structure similar to 17- β -estradiol. These isoflavones are generally found in legume family plants like peanuts, soybeans, green beans, and chickpeas. A diet with high isoflavones content shows various biological advantages like maintaining cognitive function, chemopreventive, and anti-osteoporosis [2]. Biochanin A is a

naturally available isoflavone widely found in soy, red clover, chickpea, and various plants [3,4]. The compound biochanin A exhibits various biological and pharmacological properties such as anti-inflammatory, anti-microbial, anti-cancer, anti-oxidant, hepatoprotective, and neuroprotective [5-10]. Globally, in women, breast cancer incidences are more common, and ICMR reported approximately 1.4 lakh new breast cancer instances in India [11], and the age group of people affected was between 20 to 60 years [12]. So, breast cancer treatment is done through chemotherapy that focuses on the function of receptors. The estrogen receptor (ER) exhibits the function of breast cancer initiation and progression, and the progesterone receptor (PR) was generally over-expressed in breast cancer [13,14]. The overexpression of progesterone receptor and estrogen receptor leads to a prognosis of breast cancer growth and exhibits good odds of response for hormonal therapy [15]. In triple-negative breast cancer (TNBC), epidermal growth factor receptor (EGFR) plays a major role, and the alternative treatment for TNBC was very narrow as they are differentiated phenotypically as PR-negative, ER-negative, and HER-2 negative [16]. Therefore the inhibition of epidermal growth factor receptors can be an effective treatment strategy. The chemokine ligand 18 (CCL18) can be considered a target protein in breast cancer as the chemokine was derived from tumor-associated macrophages (TAMs) to appropriate breast cancer metastasis [17]. B-cell lymphoma 2 (BCL2) is a group of a protein family that acts as an anti-apoptotic protein and is reported as a prognostic marker in the inner mitochondrial membrane [18]. The metastatic pathway in breast cancer was associated with cell cycle regulators, transcriptional factors, and tyrosine kinase. These proteins interact and inhibit HSP90, which shows a potent treatment for breast cancer [19]. An emerging therapeutic target in human breast cancer was glycogen synthase kinase-3 (GSK-3). Its inhibition reduces the viability of breast cancer cells [20], and mutation in the gene that undergoes tumor suppressor PTEN gene deleted on chromosome 10 that leads to uncontrolled PI3K pathway activation. In these PI3Ks downstream effectors, PDK1 (3-phosphoinositide-dependent protein kinase 1) plays a major role in cancers [21]. The p21-activated kinase 4 (PAK4) in breast cancer is a little more interesting than PAK4 is overexpressed in primary human breast cancer and breast cancer cell lines and rat tumor samples. Still, in the case of normal tissues, it was barely detected [22]. So these different breast cancer proteins can be potential drug targets for breast cancer treatment.

In this current study, density functional theory (DFT) was performed for biochanin A to analyze the stable molecular shape, reactive nature, charge transfer stabilization interactions, and potential reactive sites [23], and the molecular docking simulations have been performed to analyze the ligand interactions with the target protein and to analyze the binding affinity of protein-ligand interaction [24], and ADMET evaluation was performed to analyze the safety profile of the lead molecule. Because of these considerations, Biochanin A was subjected to the combination of DFT quantum chemical investigation and Molecular docking simulation that would be further helpful for in-vitro and in-vivo studies. The DFT investigation was performed with the Gaussian 09W program package, and the molecular docking simulation was done using PyRx 0.8 software. This computer-aided investigation provides a clear analysis of the lead molecule against breast cancer, which could be useful for drug discovery through *in-vitro* and *in-vivo* studies.

2. Materials and Methods

2.1. Retrieval of a lead molecule.

The 3D crystallographic structure of the lead molecule biochanin A was retrieved from the online database PubChem (<https://pubchem.ncbi.nlm.nih.gov/>). The biochanin A (CID: 5280373) and control tamoxifen (CID: 2733526) was retrieved in “.sdf” format. The canonical SMILES were utilized for the evaluation of drug-likeness properties. (SMILES: COC1=CC=C(C=C1)C2=COC3=CC(=CC(=C3C2=O)O)O).

2.2. DFT calculations using Gaussian 09W.

In the Gaussian 09W package, the DFT/B3LYP with 6-311++G(d,p) level was used to optimize the initial geometry of biochanin A [25]. The visualizer tool Gauss View 05 was utilized to visualize the optimized molecular structure, FMOs, and MEP surface [26]. A HOMO-LUMO study was performed to analyze the charge transfer throughout the biochanin A. The chemical potential and chemical hardness were obtained from values of the highest occupied molecular orbital (HOMO) and lowest unoccupied molecular orbital (LUMO). Natural population analysis was done to investigate the natural energies of an individual atom of the lead molecule.

2.3. Molecular docking simulation.

The target proteins were downloaded from the RCSB Protein Data Bank (PDB) online database (<https://www.rcsb.org/>). The ten breast cancer target proteins HER-2, HSP90, BCL2, CCL18, ER α , EGFR, GSK3, PDK1, PR, and PAK4 (PDB ID: 2IOK, 2VCJ, 4AQ3, 4MHE, 6WOK, 2J6M, 1GNG, 1UU7, 4OAR and 2X4Z) were retrieved and by using the PDB ID of these target proteins, active site region was analyzed through CASTp 3.0 (Computed Atlas of Surface Topography of proteins) online tool (<http://sts.bioe.uic.edu/>). Then the retrieved proteins were processed using BIOVIA Discovery studio 2020 software by removing the ligands, hetatms, and water molecules. The processed proteins were then saved in “.pdb” format. Docking was then performed using PyRx 0.8 tool. Initially, the lead molecule biochanin A was imported in “.sdf” format and was minimized and converted into “.pdbqt” file. The target proteins were then loaded on the workspace and made into macromolecules. The grid box was made at the active site of target proteins, and a docking simulation was performed. Finally, the docking scores were analyzed and saved in “.csv” format.

2.4. Analysis of protein-ligand interaction.

The output file of molecular docking was used to visualize the interactions between the protein and ligand. BIOVIA Discovery Studio 2020 was used to visualize the interaction of the protein-ligand. The protein structure was imported first on the graphical window then the ligand molecule was utilized from the output of vina. Once the ligand and protein were loaded on the graphical window, interactions were made, and the type of bond, bond distances, and amino residues involved in the interactions was analyzed. Then the presence of ligands at the receptor region of the protein and interactions in 2D and 3D was saved in “.jpeg” format.

2.5. Pharmacokinetic evaluation.

The physiochemical (Lipinski's Rule of Five) and pharmacokinetic properties (ADMET) of the lead compound biochanin A were evaluated using the pkCSM online tool (<http://biosig.unimelb.edu.au/pkcsm/prediction>). The retrieved canonical SMILES were loaded on the pkCSM tool, the drug-likeness evaluation was processed, and the safety profile of biochanin A was analyzed.

3. Results and Discussion

3.1. Frontier molecular orbitals (FMO).

Initially, the lead molecule biochanin A was optimized using DFT method through B3LYP with a 6-311G++(d,p) basis set. The molecule's interaction with other species was determined through the evaluation of frontier molecular orbital (FMO). The highest occupied molecular orbital (HOMO) and the lowest unoccupied molecular orbital (LUMO) are the frontier molecular orbital. HOMO is a nucleophile that provides electrons, and LUMO is an electrophile that receives electrons [27,28]. The FMO evaluation gives the data on the energy gap between the HOMO and LUMO states, which helps determine a molecule's stability. A molecule that has a lower energy gap is highly polarisable and has better chemical reactivity. It is said to be softer, whereas better stability and high chemical hardness were seen in molecules with a greater energy gap [29,30]. The global reactivity descriptors, electron affinity (A), ionization potential (I), chemical potential (μ), electronegativity (χ), softness (S), global hardness (η), and electrophilicity index (ω) may be estimated using Koopmans' theorem and the energies of HOMO and LUMO of the lead molecule biochanin A. The FMO plot obtained for biochanin A is shown in figure 1. Table 1 shows the lead molecule's calculated EHOMO, ELUMO, and the energy gap (ELUMO-EHOMO). According to Koopman's theorem, the ionization potential (I) is the negative energy of HOMO, and electron affinity (A) is the negative energy of LUMO. Then the electronegativity (χ) is defined by $\chi = (I+A)/2$, and chemical potential (μ) is a negative of electronegativity $\mu = -(I+A)/2$. Electronegativity and chemical potential are estimated from the values of electron affinity and ionization potential. The chemical hardness (η) is defined by $\eta = (I-A)/2$, and chemical softness (S) was the inverse of chemical hardness $S = 1/\eta$, and the values are tabulated in table 1. The tabulated values of lead molecule biochanin A shows that it has better chemical strength and stability. The great stream of electrons in the middle of the donor (HOMO) and the acceptor (LUMO) brings about a lowering of energy considered to be the electrophilicity index [31]. Biochanin A has the electrophilicity index of $\omega = \mu^2 / 2\eta = 3.8270\text{eV}$.

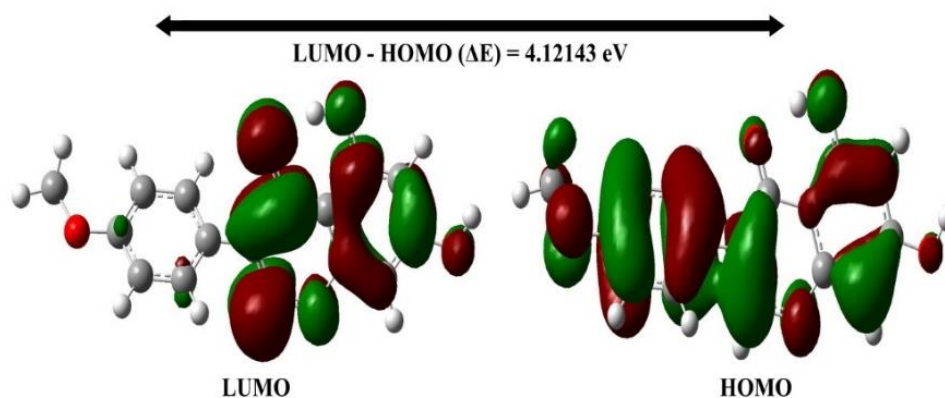


Figure 1. The energy band gap between LUMO and HOMO of the lead molecule Biochanin A.

Table 1. Calculated FMOs and related molecular properties values of Biochanin A using DFT.

S.No.	Parameters (eV)	B3LYP/6-311++G(d,p) basis set
1	ELUMO	-1.91078
2	EHOMO	-6.03221
3	$\Delta(\text{ELUMO} - \text{EHOMO})$	4.12143
4	ELUMO+1	-1.15321
5	EHOMO-1	-6.62976
6	ELUMO+1 - EHOMO-1	5.476557
7	Electron Affinity (A)	1.91078
8	Ionization Potential (I)	6.03221
9	Chemical Hardness (η)	2.0607
10	Chemical softness (S)	0.4852
11	Chemical Potential (μ)	-3.97149
12	Electronegativity (γ)	3.97149
13	Electrophilicity Index(ω)	3.8270

3.2. Molecular electrostatic potential (MEP).

Molecular electrostatic potential (MEP) is utilized to analyze the lead molecule's physical and chemical properties depending on molecular form, size, and electrostatic potential based on the color grading [31]. Based on electrophilic and nucleophilic features, a molecule's chemical stability and reactivity can be analyzed through MEP. For biochanin A, MEP map and contour surface were created using B3LYP techniques at the 6-311++G(d,p) level. The MEP map of biochanin is shown in figure 2a, and contour plots of the lead molecule are displayed in figure 2b. The various colors on the surface display the nucleophilic and electrophilic properties of the lead molecule. The higher nucleophilic potential was denoted in blue color, and the higher electrophilic potential was denoted in red color. The drop of electrical potential will be in the color order: blue < cyan < green < yellow < orange < red. The color codes for lead molecule ranges between -6.831×10^{-2} to 6.831×10^{-2} . The red color in MEP structure indicates the electron-rich region, and the blue color indicates the electron-poor region of the molecule. The polarization effect of the molecule is visible. The negative potential regions of the molecule are positioned slightly over oxygen atoms O4 and O12, hydrogen atoms H27 and H25, and one carbon atom C14, and the positive potential regions were located all over other atoms. As a result, locations with greater negative electronegative potential and a greater positive electrostatic potential remain additional attractive to nucleophilic and electrophilic species.

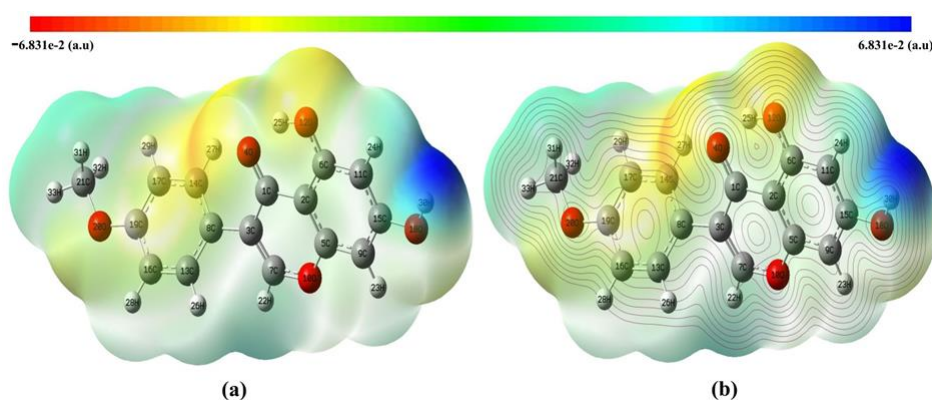


Figure 2. a)Molecular electrostatic potential. b)contour plot surface of Biochanin-A.

3.3. Mulliken charge population analysis.

The atomic charges play a vital role in the application of quantum chemical calculations and are expected to alter the variables like polarizability, vibrational spectra, dipole moment,

electronic structure, and various properties of a molecular system [32]. The donor and acceptor pairs suggested the charge distribution over the atoms involved in the charge transfer process. The atomic charges for the lead molecule biochanin A were determined at the gas phase using Mulliken population analysis by the B3LYP/6-311G++(d,p) method, and the results are displayed in table 2. The charge distribution of the molecule has a significant effect on vibrational spectra. The total atomic charge values determined using Mulliken population analysis with the optimized geometry are shown in figure 3. Figure 3 reveals that all the hydrogen atoms have a net positive charge and all the oxygen atoms show negative charges. Except for C2, C3, C8, C11, and C17, all other carbon atoms possess a negative charge. The atomic charges show that lead molecule has more charge delocalization [33].

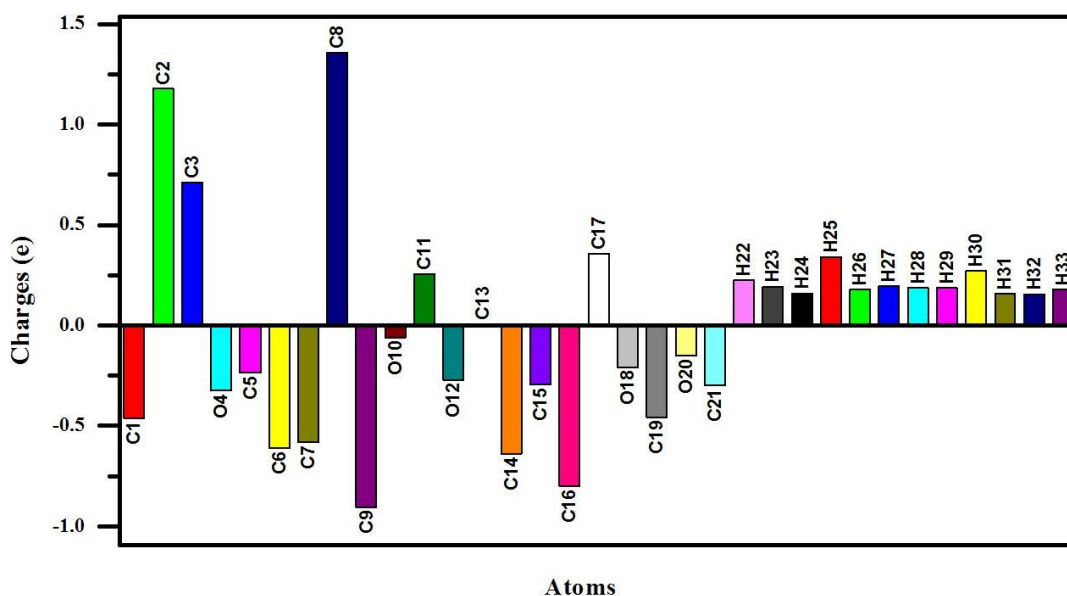


Figure 3. Mulliken atomic charge distribution of lead molecule Biochanin-A.

Table 2. Mulliken atomic charges of the lead molecule Biochanin-A.

Atom	Mulliken Atomic Charge	Atom	Mulliken Atomic Charge
C1	-0.46121	O18	-0.20843
C2	1.17858	C19	-0.4567
C3	0.712205	O20	-0.15102
O4	-0.32424	C21	-0.29832
C5	-0.23638	H22	0.224397
C6	-0.61099	H23	0.193132
C7	-0.58224	H24	0.160323
C8	1.357735	H25	0.341055
C9	-0.90345	H26	0.178104
O10	-0.06006	H27	0.195325
C11	0.256872	H28	0.18638
O12	-0.27242	H29	0.185295
C13	0.00837	H30	0.270284
C14	-0.6376	H31	0.156779
C15	-0.29432	H32	0.155115
C16	-0.79973	H33	0.179154
C17	0.358019		

3.4. Natural population analysis.

The natural population analysis was utilized to reveal the distribution of electrons in various sub-shells of an atomic orbital. Natural energies of all the atoms of the lead molecule were tabulated in table 3, as also the accumulation of electrons in the core, valance, and Rydberg sub-shells of biochanin A. The tabulated natural charges reveal that carbon atoms C1,

C5, C6, C7, C15, and C19 have good electro positivity, whereas other carbon atoms possess electro negativity. All the hydrogen atoms gained electropositive charges, and all oxygen atoms showed electronegative charges.

Table 3. Natural population charges of the lead molecule Biochanin-A.

Atom No.	Natural charge (e)	Natural population (e)			
		Core	Valence	Rydberg	Total (e)
C1	0.51409	1.99887	3.45051	0.03653	5.48591
C2	-0.27	1.99885	4.25611	0.01503	6.27
C3	-0.16964	1.99877	4.15122	0.01966	6.16964
O4	-0.64467	1.99974	6.63169	0.01323	8.64467
C5	0.37486	1.99874	3.604	0.0224	5.62514
C6	0.40566	1.99885	3.56794	0.02755	5.59434
C7	0.23645	1.99886	3.74149	0.02319	5.76355
C8	-0.10699	1.99906	4.08708	0.02085	6.10699
C9	-0.3349	1.99898	4.31711	0.01881	6.3349
O10	-0.47033	1.99968	6.4523	0.01835	8.47033
C11	-0.35033	1.99899	4.33381	0.01753	6.35033
O12	-0.67007	1.99974	6.65645	0.01388	8.67007
C13	-0.16071	1.99891	4.14566	0.01613	6.16071
C14	-0.1317	1.9989	4.11577	0.01703	6.1317
C15	0.36938	1.99886	3.60737	0.0244	5.63062
C16	-0.24364	1.9991	4.22584	0.01869	6.24364
C17	-0.29117	1.99908	4.27615	0.01593	6.29117
O18	-0.65863	1.99975	6.64656	0.01233	8.65863
C19	0.32926	1.99878	3.64906	0.0229	5.67074
O20	-0.54077	1.99971	6.52271	0.01835	8.54077
C21	-0.20535	1.99922	4.19022	0.01592	6.20535
H22	0.19781	0	0.8001	0.00209	0.80219
H23	0.241	0	0.757	0.002	0.759
H24	0.21743	0	0.77996	0.00261	0.78257
H25	0.50513	0	0.48798	0.00688	0.49487
H26	0.20291	0	0.79484	0.00225	0.79709
H27	0.22075	0	0.77585	0.0034	0.77925
H28	0.21841	0	0.77968	0.00191	0.78159
H29	0.21206	0	0.78593	0.002	0.78794
H30	0.47173	0	0.52374	0.00453	0.52827
H31	0.17076	0	0.82676	0.00248	0.82924
H32	0.16939	0	0.82814	0.00247	0.83061
H33	0.19197	0	0.80663	0.00139	0.80803

3.5. Molecular docking simulation.

The active site region of the target proteins was initially analyzed using the online tool CASTp. The docking analysis further utilized these binding regions of the breast cancer proteins.

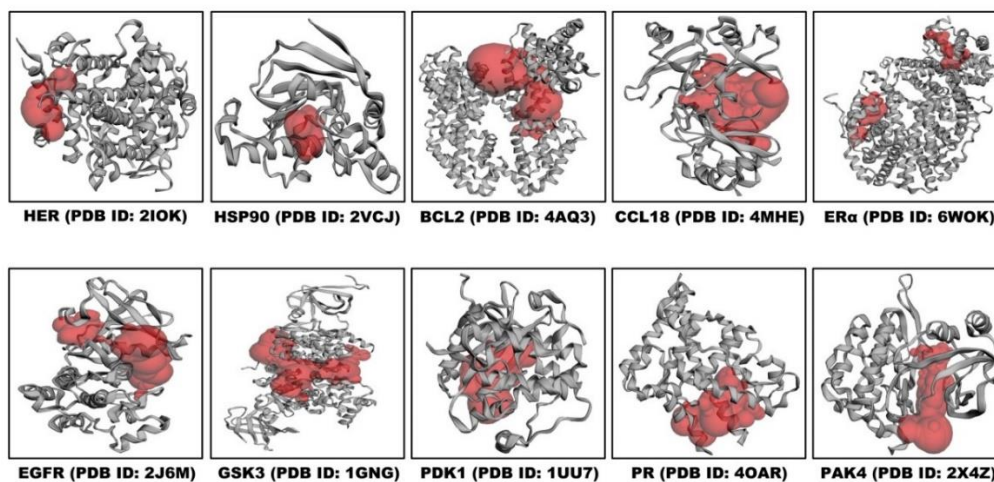


Figure 4. The active site regions of breast cancer target proteins.

The red color region shown in figure 4 denotes the active region of the proteins where the binding of the lead compound with proteins could be better. The molecular docking simulation of the lead molecule against the breast cancer target proteins was performed utilizing the tool PyRx 0.8 version. The docking scores of the lead molecule and standard tamoxifen (CID: 2733526) against the target proteins were tabulated in table 4. This study used tamoxifen as a standard for docking studies against target proteins due to previously reported inhibitory activity against breast cancer [34].

Tamoxifen is a breast cancer drug that is commercially available that binds with the receptors of breast cancer proteins, and it prevents the uncontrolled proliferation of cells. The biochanin A with the target proteins showed a good binding affinity with binding scores greater than -7Kcal/mol. The binding scores of the lead molecule range between -7.1Kcal/mol to -9.2Kcal/mol. The highest binding score was observed against the target protein HER-2 (PDB ID: 2IOK) with a binding affinity of -9.2Kcal/mol. The lead molecule has shown better binding affinity against all the target proteins when compared with the standard drug tamoxifen. These docking results showed that biochanin A has a better binding affinity with all the target proteins at their active site regions.

Table 4. The docking scores of Biochanin-A and Tamoxifen against target proteins.

S.No	Protein	PDB ID	Binding Affinity (Kcal/mol)	
			Biochanin A	Tamoxifen
1	HER-2	2IOK	-9.2	-7.1
2	HSP90	2VCJ	-7.7	-5.5
3	BCL2	4AQ3	-8.3	-7.7
4	CCL18	4MHE	-7.7	-6.7
5	ER α	6WOK	-7.9	-6.9
6	EGFR	2J6M	-7.7	-7.1
7	GSK3	1GNG	-8.5	-7.9
8	PDK1	1UU7	-8.0	-7.6
9	PR	4OAR	-7.9	-7.8
10	PAK4	2X4Z	-7.1	-6.8

3.6. Interpretation of protein-ligand interaction.

The interactions between the lead compound and the breast cancer target proteins were visualized using BIOVIA Discovery studio 2020 software. During the visualization, the type of bond and bond distances were analyzed.

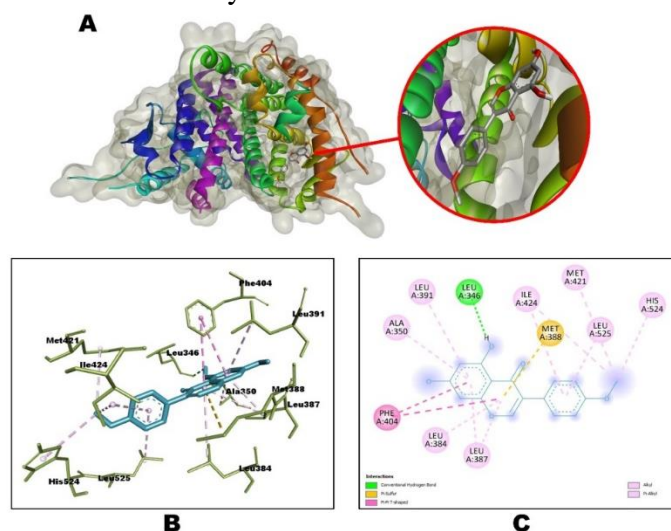


Figure 5. Interaction of Biochanin A with HER-2. (A)The close depiction of active regions of target protein HER-2 with Biochanin A. (B)3D interaction of Biochanin A at the active site of the target protein. (C)2D interaction of Biochanin A with HER-2, including type of bond.

The interaction between the biochanin A and the target molecules is shown in figure 5 to figure 14. The lead compound biochanin A with the target protein HER-2 formed one (1) acceptor hydrogen bond interaction with the amino residue LEU346 with the bond distance of 2.76253 Å, one (1) Pi-Sulfur interaction with MET388 at 5.98652 Å and two (2) Pi-Pi T-shaped, two (2) Alkyl and eight (8) Pi-Alkyl hydrophobic bond interactions with PHE404 (2), MET421, ILE424, HIS524, LEU384, LEU387, ALA350, LEU387, LEU391, ILE424 and LEU525 at bond distances 5.61252 Å, 4.92608 Å, 4.71274 Å, 4.99488 Å, 4.62736 Å, 5.48925 Å, 5.33652 Å, 5.05572 Å, 4.19886 Å, 5.10588 Å, 4.79299 Å and 5.41542 Å respectively.

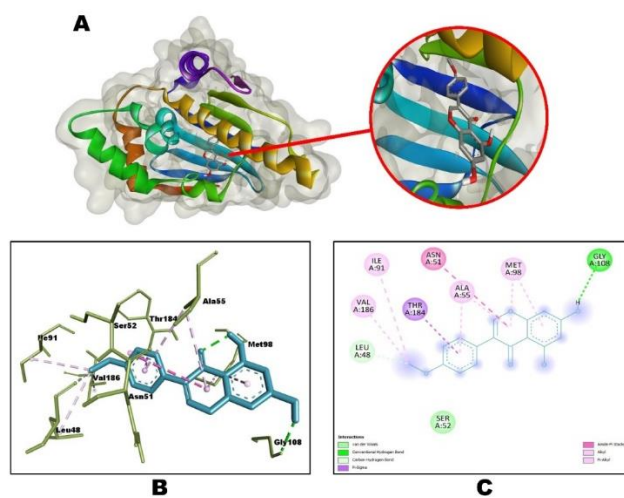


Figure 6. Interaction of Biochanin A with HSP90. (A)The close depiction of active regions of target protein HSP90 with Biochanin A. (B)3D interaction of Biochanin A at the active site of the target protein. (C)2D interaction of Biochanin A with including HSP90 type of bond.

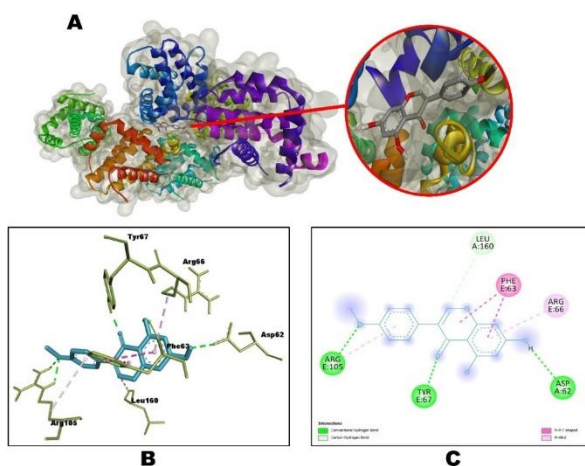


Figure 7. Interaction of Biochanin A with BCL2. (A)The close depiction of active regions of target protein BCL2 with Biochanin A. (B)3D interaction of Biochanin A at the active site of the target protein. (C)2D interaction of Biochanin A with BCL2, including type of bond.

Biochanin A with HSP90 formed one (1) acceptor conventional and one (1) acceptor carbon-hydrogen bond interaction with GLY108, LEU48 at 2.2492 Å and 3.32033 Å also, it has formed one (1) Pi-Sigma, one (1) Amide-Pi stacked, two (2) Alkyl and four (4) Pi-Alkyl hydrophobic interactions with THR184, ASN51, ILE91, VAL186, ALA55, MET98 (2) and ALA55 at 3.9692 Å, 5.4854 Å, 4.48003 Å, 4.12371 Å, 4.99358 Å, 4.93668 Å, 5.07005 Å and 5.00243 Å bond distances and also one Van der Waals force with SER52. Target protein BCL2 with lead molecule formed two (2) donor conventional, one (1) acceptor conventional, and one (1) acceptor carbon-hydrogen bond interactions with amino residues TYR67, ARG105, ASP62

and LEU160 at 1.95383 Å, 2.33464 Å, 2.50276 Å and 3.65351 Å and two (2) Pi-Pi T-shaped and two (2) Pi-Alkyl hydrophobic interactions with PHE63 (2), ARG66 and ARG105 amino residues at the bond distances of 4.67747 Å, 5.11004 Å, 4.80189 Å and 4.98223 Å.

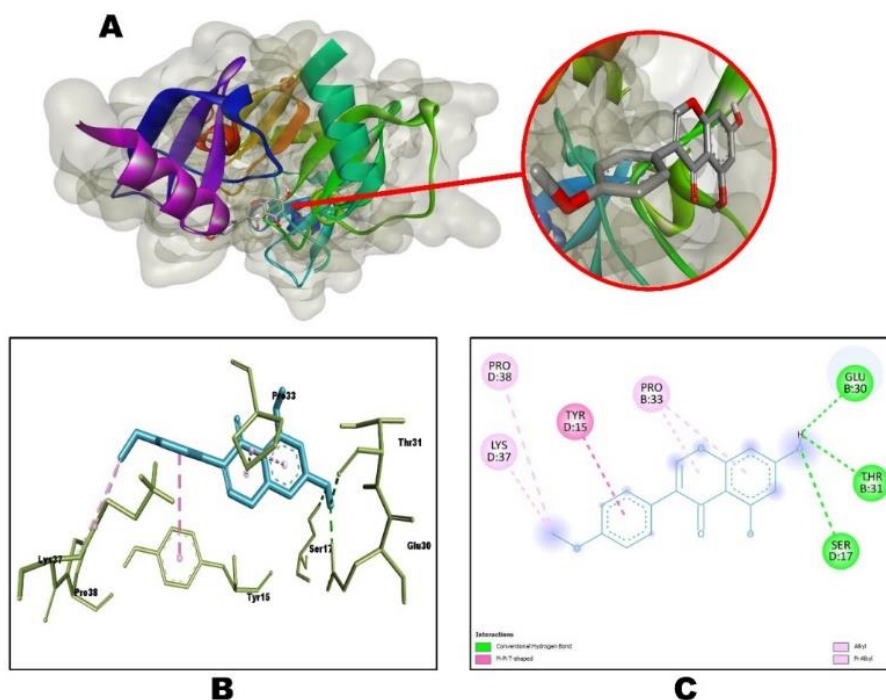


Figure 8. Interaction of Biochanin A with CCL18. (A)The close depiction of active regions of target protein CCL18 with Biochanin A. (B)3D interaction of Biochanin A at the active site of the target protein. (C)2D interaction of Biochanin A with CCL18, including type of bond.

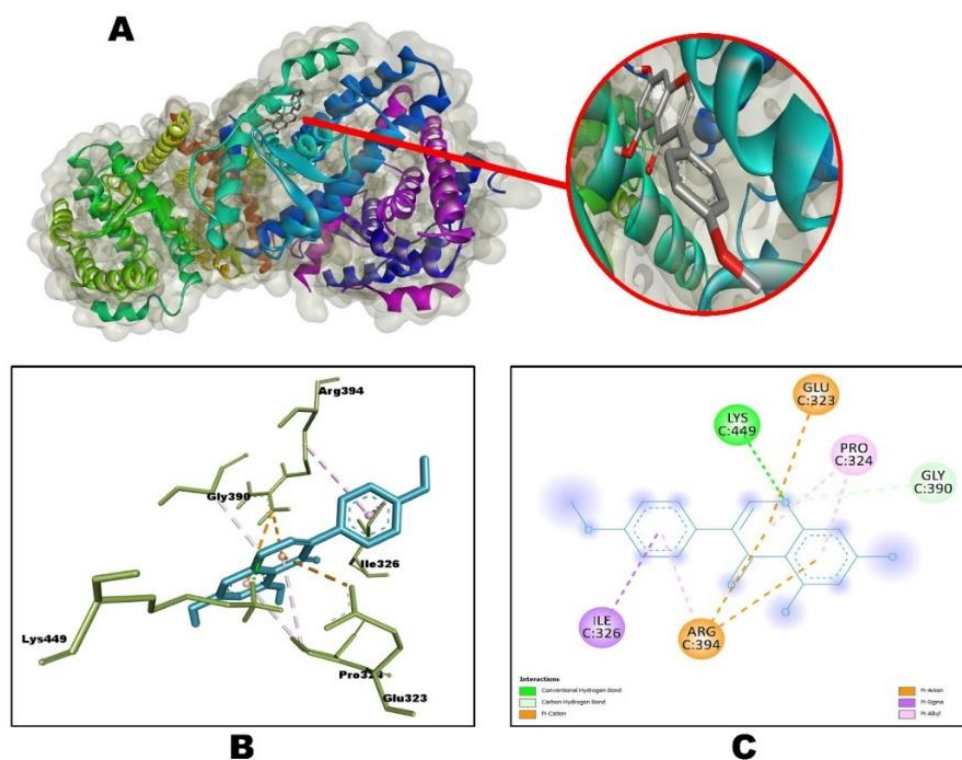


Figure 9. Interaction of Biochanin A with ERα. (A)The close depiction of active regions of target protein ERα with Biochanin A. (B)3D interaction of Biochanin A at the target protein's active site. (C)2D interaction of Biochanin A with ERα, including the type of bond.

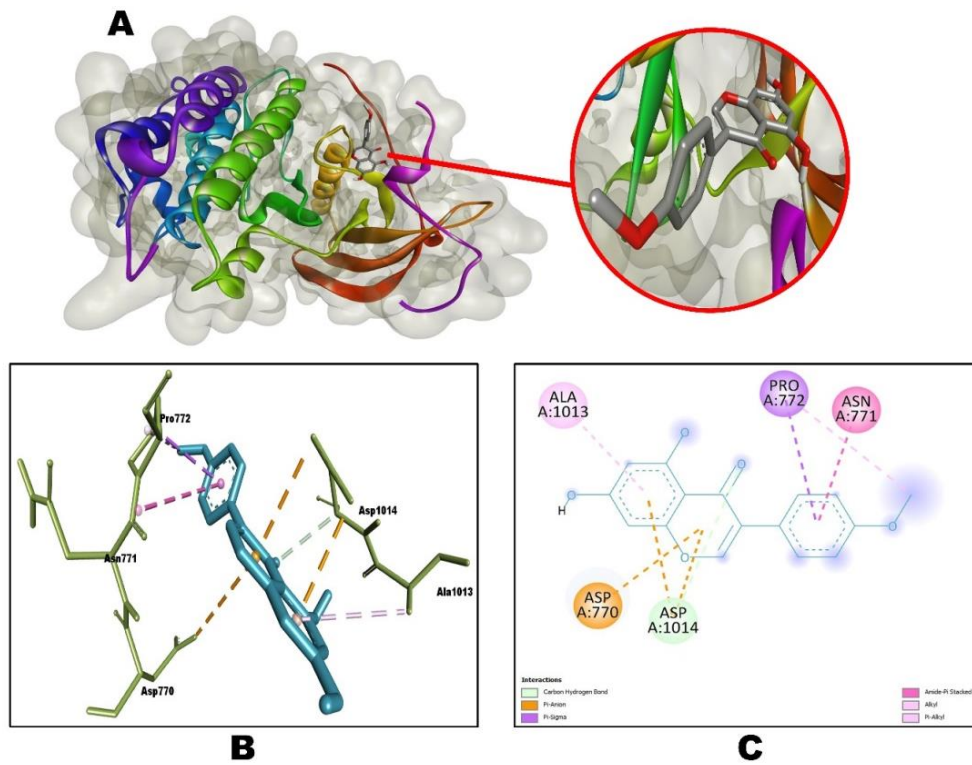


Figure 10. Interaction of Biochanin A with EGFR. (A)The close depiction of active regions of target protein EGFR with Biochanin A. (B)3D interaction of Biochanin A at the active site of the target protein. (C) 2D interaction of Biochanin A with EGFR, including the type of bond.

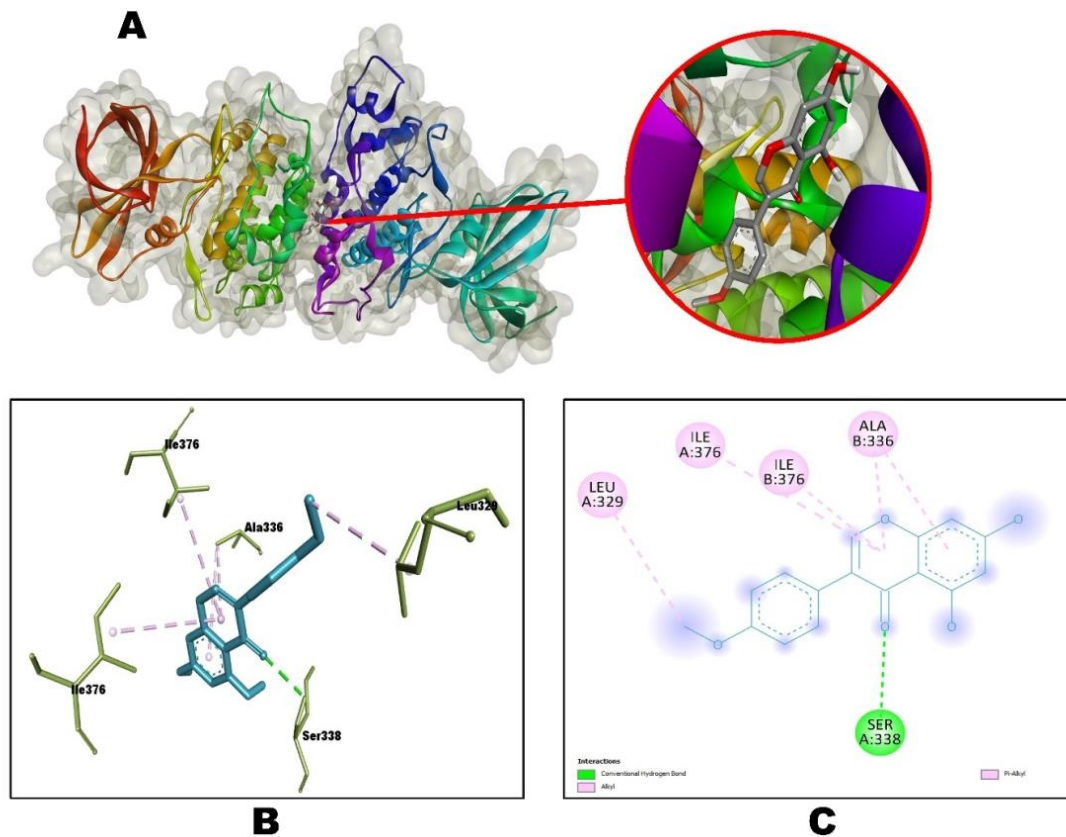


Figure 11. Interaction of Biochanin A with GSK3. (A)The close depiction of active regions of target protein GSK3 with Biochanin A. (B)3D interaction of Biochanin A at the active site of the target protein. (C) 2D interaction of Biochanin A with GSK3, including the type of bond.

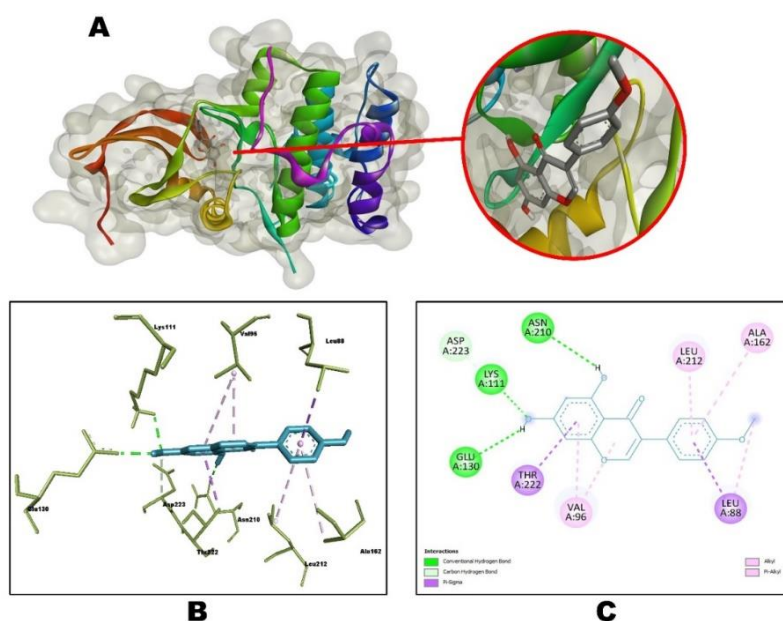


Figure 12. Interaction of Biochanin A with PDK1. (A)The close depiction of active regions of target protein PDK1 with Biochanin A. (B)3D interaction of Biochanin A at the active site of the target protein. (C) 2D interaction of Biochanin A with PDK1, including type of bond.

Chemokine ligand 18 with the lead molecule formed three (3) conventional hydrogen bond interactions at one (1) donor and two (2) acceptor regions with the amino residues SER17, GLU30, and THR31 at 2.96426 Å, 2.22134 Å, and 2.82323 Å and one (1) Pi-Pi T-shaped, two (2) Alkyl and two (2) Pi-Alkyl hydrophobic bond interactions with TYR15, LYS37, PRO38 and PRO33 (2) at distances 4.82763 Å, 4.24281 Å, 5.21213 Å, 4.41926 Å, and 5.18851 Å respectively. Biochanin A with protein of target ER α formed one (1) donor conventional and one (1) donor carbon-hydrogen bond interactions with LYS449 and GLY390 at 2.06249 Å and 3.5084 Å. Other interactions include two (2) Pi-Cation and one (1) Pi-Anion electrostatic interaction with ARG394 (2) and GLU323 at 4.11738 Å, 4.61509 Å, and 4.28278 Å and one (1) Pi-Sigma and three (3) Pi-Alkyl hydrophobic interactions with amino residues ILE326, PRO324(2) and ARG394 at 3.85408 Å, 4.46702 Å, 4.04937Å and 5.11089 Å bond distances.

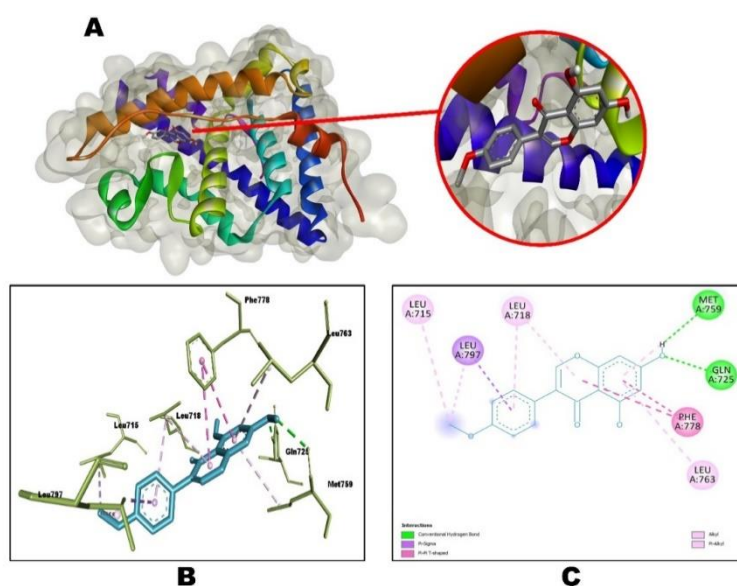


Figure 13. Interaction of Biochanin A with PR. (A)The close depiction of active regions of target protein PR with Biochanin A. (B)3D interaction of Biochanin A at the active site of the target protein. (C)2D interaction of Biochanin A with PR, including the type of bond.

EGFR with biochanin A formed one (1) donor carbon-hydrogen bond interaction with ASP1014 at 3.27799 Å, three (3) Pi-Anion electrostatic interactions with ASP770 and ASP1014 (2) at 4.67942 Å, 3.71759 Å and 3.9324 Å and one (1) Pi-Sigma, one (1) Amide-Pi stacked, one (1) Alkyl and one (1) Pi-Alkyl hydrophobic interactions with amino residues PRO772, ASN771, PRO772 and ALA1013 at distances 3.67546 Å, 5.15637 Å, 4.69068 Å and 4.41897 Å. The target protein GSK3 with lead molecule formed one (1) donor conventional hydrogen bond with SER338 at 2.72191 Å, one (1) Alkyl hydrophobic with LEU329 at 4.42176 Å and four (4) Pi-Alkyl hydrophobic interactions with ILE376 (2) and ALA336 (2) at 5.26194 Å, 5.10937 Å, 4.49044 Å, and 5.23435 Å bond distances. Biochanin A with PDK1 formed one (1) donor conventional, two (2) acceptor conventional, and one (1) donor carbon-hydrogen bond interactions with LYS111, ASN210, GLU130, and ASP223 at 2.3571 Å, 2.67804 Å, 2.18403 Å and 3.51741 Å distances and also other interactions such as two (2) Pi-Sigma, one (1) Alkyl and four (4) Pi-Alkyl hydrophobic interactions with 3.58282 Å, 3.8738Å, 4.54554 Å, 4.1264 Å, 5.31773 Å, 5.45654 Å, and 5.26051 Å distances. PR with biochanin A formed one (1) donor and one (1) acceptor conventional hydrogen bond interactions with amino residues GLN725 and MET759 at 1.95644Å and 2.53322 Å and one (1) Pi-Sigma, two (2) Pi-Pi T-shaped, two (2) Alkyl and four (4) Pi-Alkyl with LEU797, PHE778 (2), LEU715, LEU797, LEU718, MET759, LEU763 and LEU718 at distances 3.84187 Å, 5.17642 Å, 4.81135 Å, 5.06561 Å, 5.35689 Å, 5.20599 Å, 5.3991 Å, 5.288887 Å and 5.24988 Å respectively. Biochanin A with PAK4 protein formed two (2) acceptor conventional hydrogen bond interactions and one (1) donor carbon-hydrogen bond interaction with ARG534, ASP510, and TYR515 at 1.91416 Å, 2.51712 Å, and 2.51133 Å and one (1) Pi-Sigma, one (1) Alkyl and two (2) Pi-Alkyl hydrophobic interactions with PRO514, MET526 and LYS536 (2) at 3.58765Å, 5.26447Å, 5.48379Å, and 4.31504Å bond distances. The lead molecule Biochanin A has shown a good binding effect with the target proteins at the binding regions. Depending on effective binding ability, strong hydrogen bond interactions and other bond interactions with the amino acids located at the active sites of the target proteins show the good anti-cancer potential of biochanin A as an effective drug for the treatment of breast cancer.

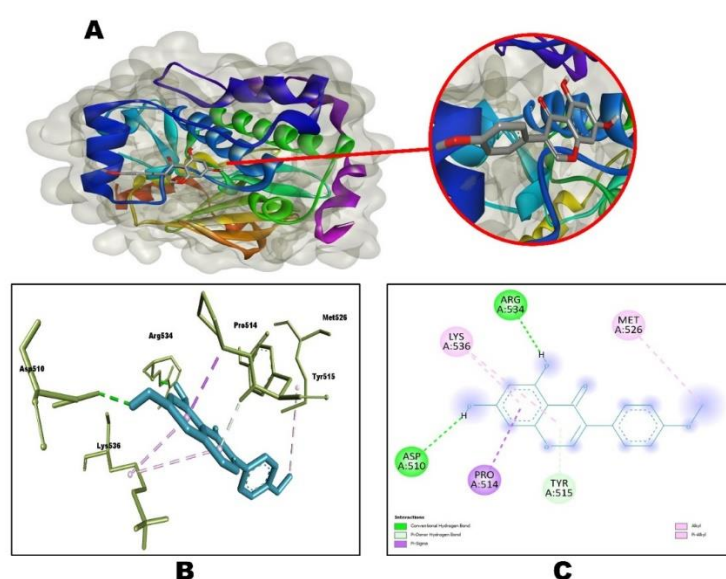


Figure 14. Interaction of Biochanin A with PAK4. (A)The close depiction of active regions of target protein PAK4 with Biochanin A. (B)3D interaction of Biochanin A at the active site of the target protein. (C)2D interaction of Biochanin A with PAK4, including type of bond.

3.7. Pharmacokinetic evaluation.

The drug-likeness properties of the lead molecule biochanin A were evaluated based on the physiochemical and ADMET (absorption, distribution, metabolism, excretion, and toxicity) characteristics. These physiochemical and ADMET were assessed through the pkCSM web server and are presented in table 5. According to Lipinski's rule, the molecular weight should be less than 500 Dalton, the rotatable bonds and hydrogen bond acceptors should be less than 5, and the hydrogen bond donor and partition coefficient should be lesser than 5. The molecular weight of the lead molecule was 284.267 Dalton, and partition co-efficient LogP was assessed to be 2.8798. The lead molecule biochanin A showed no violation of Lipinski's rule and can be utilized as a drug compound after clinical studies [35]. Based on the pharmacokinetic evaluation, the water solubility was analyzed to be -3.735, the Caco2 permeability range was 0.897, skin permeability was valued at -2.737, and the molecule biochanin A showed better human intestinal absorption with the range of 93.028. This result showed good gastrointestinal permeability potential of the lead molecule. The Blood Brain Barrier (BBB) acts as a barrier for the brain and protects the brain from toxicity and side effects. The BBB permeability range shows that the lead molecule can partially penetrate through the blood-brain barrier, and the CNS permeability range of the lead molecule was assessed as -2.115. Biochanin A was not a CYP2D6 substrate, CYP2D6, and CYP3A4 inhibitor, but a CYP3A4 substrate. The total clearance range was assessed to be 0.247, and the lead molecule was not renal OCT2 substrate. The toxicity assessment was important during drug discovery, and oral rat acute toxicity (LD50) of the lead molecule biochanin A was analyzed to be 1.851, and biochanin A was not hepatotoxic, with no skin sensitization and not hERG I and II inhibitor. This drug-likeness evaluation showed a good safety profile of the lead compound biochanin A, which can be considered a potent drug compound against breast cancer.

Table 5. Pharmacokinetic parameters of lead molecule biochanin A.

Properties	Parameter	Value
Physiochemical properties	Molecular Weight (Da)	284.267
	LogP	2.8798
	No. of Rotatable Bonds	2
	No. of H-Bond Acceptors	5
	No. of H-Bond Donors	2
Absorption	Water solubility	-3.735
	Caco2 permeability	0.897
	Intestinal absorption (human)	93.028
	Skin Permeability	-2.737
Distribution	BBB permeability	-0.221
	CNS permeability	-2.115
Metabolism	CYP2D6 substrate	No
	CYP3A4 substrate	Yes
	CYP2D6 inhibitor	No
	CYP3A4 inhibitor	No
Excretion	Total Clearance	0.247
	Renal OCT2 substrate	No
Toxicity	Hepatotoxicity	No
	Skin Sensitization	No
	hERG I inhibitor	No
	hERG II inhibitor	No
	Oral Rat Acute Toxicity (LD50)	1.851

4. Conclusions

The theoretical DFT method was used to optimize and characterize the structural properties of the lead molecule Biochanin A. According to FMO evaluation, molecular

reactivity, intramolecular charge transfer, and kinetic stability were the factors that influence the bioactivity of Biochanin A, and the energy gap was computed to be $\Delta E = 4.12143$ eV. The Mulliken charge distribution and natural population analysis were performed, and the reactive sites and electron distribution of Biochanin A were validated. The docking studies revealed the binding affinity of the lead molecule against the breast cancer target proteins and showed the highest docking score of -9.2 Kcal/mol, and the type of interactions between the ligand and active site of proteins was analyzed. The physicochemical and pharmacokinetic studies show the drug-likeness characteristics of Biochanin A with no violation of Lipinski's rule and computed as non-toxic is theoretical evaluation will be useful for further in-vitro and in-vivo studies in drug development, and the lead molecule biochanin A can be considered a potent drug for the treatment of breast cancer.

Funding

This research received no external funding.

Acknowledgments

This research has no acknowledgment.

Conflicts of Interest

The authors declare no conflict of interest.

References

1. Mujeeb, F.; Bajpai, P.; Pathak, N. Phytochemical Evaluation, Antimicrobial Activity, and Determination of Bioactive Components from Leaves of *Aegle marmelos*. *BioMed Research International* **2014**, *2014*, <https://doi.org/10.1155/2014/497606>.
2. Ko, K.P. Isoflavones: chemistry, analysis, functions and effects on health and cancer. *Asian Pacific journal of cancer prevention*. *Asian Pacific Journal of Cancer Prevention* **2014**, *15*, 7001-7010, <https://doi.org/10.7314/APJCP.2014.15.17.7001>.
3. Yu, C.; Zhang, P.; Lou, L.; Wang, Y. Perspectives Regarding the Role of Biochanin A in Humans. *Frontiers in Pharmacology* **2019**, *10*, <https://doi.org/10.3389/fphar.2019.00793>.
4. Li, S.; Wang, J.; Yu, Y.; Zheng, B.; Ma, J.; Kou, X.; Xue, Z. Investigation on the mechanisms of biochanin A alleviate PM10-induced acute pulmonary cell injury. *Ecotoxicology and Environmental Safety* **2021**, *228*, <https://doi.org/10.1016/j.ecoenv.2021.112953>.
5. Kole, L.; Giri, B.; Manna, S.K.; Pal, B.; Ghosh, S. Biochanin-A, an isoflavon, showed anti-proliferative and anti-inflammatory activities through the inhibition of iNOS expression, p38-MAPK and ATF-2 phosphorylation and blocking NF κ B nuclear translocation. *European Journal of Pharmacology* **2011**, *653*, 8-15, <https://doi.org/10.1016/j.ejphar.2010.11.026>.
6. Sithisarn, P.; Michaelis, M.; Schubert-Zsilavecz, M.; Cinatl, J. Differential antiviral and anti-inflammatory mechanisms of the flavonoids biochanin A and baicalein in H5N1 influenza A virus-infected cells. *Antiviral Research* **2013**, *97*, 41-48, <https://doi.org/10.1016/j.antiviral.2012.10.004>.
7. Singh, G.; Thaker, R.; Sharma, A.; Parmar, D. Therapeutic effects of biochanin A, phloretin, and epigallocatechin-3-gallate in reducing oxidative stress in arsenic-intoxicated mice. *Environmental Science and Pollution Research* **2021**, *28*, 20517-20536, <https://doi.org/10.1007/s11356-020-11740-w>.
8. Rahman, M.S.; Imran, K.M.; Hossain, M.; Lee, T.-J.; Kim, Y.-S. Biochanin A induces a brown-fat phenotype via improvement of mitochondrial biogenesis and activation of AMPK signaling in murine C3H10T1/2 mesenchymal stem cells. *Phytotherapy Research* **2021**, *35*, 920-931, <https://doi.org/10.1002/ptr.6845>.
9. Derangula, M.; Panati, K.; Narala, R.V. Biochanin A Ameliorates Ovalbumin-induced Airway Inflammation through Peroxisome Proliferator-Activated Receptor-Gamma in a Mouse Model. *Endocrine, Metabolic & Immune Disorders - Drug Targets* **2021**, *21*, 145-155, <https://doi.org/10.2174/1871530320666200503051609>.
10. Wu, Q.; Shang, Y.; Shen, T.; Liu, F.; Zhang, W. Biochanin A protects SH-SY5Y cells against isoflurane-induced neurotoxicity by suppressing oxidative stress and apoptosis. *NeuroToxicology* **2021**, *86*, 10-18, <https://doi.org/10.1016/j.neuro.2021.06.007>.

11. Garcia-Martinez, L.; Zhang, Y.; Nakata, Y.; Chan, H.L.; Morey, L. Epigenetic mechanisms in breast cancer therapy and resistance. *Nature Communications* **2021**, *12*, 1-14, <https://doi.org/10.1038/s41467-021-22024-3>.
12. Viswanathan, T.M.; Chitradevi, K.; Zochedh, A.; Vijayabhaskar, R.; Sukumaran, S.; Kunjiappan, S.; Kumar, N.S.; Sundar, K.; Babkiewicz, E.; Maszczyk, P.; Kathiresan, T. Guanidine–Curcumin Complex-Loaded Amine-Functionalised Hollow Mesoporous Silica Nanoparticles for Breast Cancer Therapy. *Cancers* **2022**, *14*, <https://doi.org/10.3390/cancers14143490>.
13. Lainé, M.; Fanning, S.W.; Chang, Y.-F.; Green, B.; Greene, M.E.; Komm, B.; Kurlito, J.D.; Phung, L.; Greene, G.L. Lasofoxifene as a potential treatment for therapy-resistant ER-positive metastatic breast cancer. *Breast Cancer Research* **2021**, *23*, 1-12, <https://doi.org/10.1186/s13058-021-01431-w>.
14. Tzekaki, E.E.; Geromichalos, G.; Lavrentiadou, S.N.; Tsantarliotou, M.P.; Pantazaki, A.A.; Papaspyropoulos, A. Oleuropein is a natural inhibitor of PAI-1-mediated proliferation in human ER-/PR- breast cancer cells. *Breast Cancer Research and Treatment* **2021**, *186*, 305-316, <https://doi.org/10.1007/s10549-020-06054-x>.
15. Xia, L.; Zheng, Z.; Liu, J.-Y.; Chen, Y.-J.; Ding, J.; Hu, G.-S.; Hu, Y.-H.; Liu, S.; Luo, W.-X.; Xia, N.-S. Targeting Triple-Negative Breast Cancer with Combination Therapy of EGFR CAR T Cells and CDK7 Inhibition Targeting TNBC with EGFR CAR T Cells and CDK7 Inhibition. *Cancer Immunology Research* **2021**, *9*, 707-722, <https://doi.org/10.1158/2326-6066.CIR-20-0405>.
16. Singh, S.; Numan, A.; Maddiboyina, B.; Arora, S.; Riadi, Y.; Md, S.; Alhakamy, N.A.; Kesharwani, P. The emerging role of immune checkpoint inhibitors in the treatment of triple-negative breast cancer. *Drug Discovery Today* **2021**, *26*, 1721-1727, <https://doi.org/10.1016/j.drudis.2021.03.011>.
17. Huang, X.; Lai, S.; Qu, F.; Li, Z.; Fu, X.; Li, Q.; Zhong, X.; Wang, C.; Li, H. CCL18 promotes breast cancer progression by exosomal miR-760 activation of ARF6/Src/PI3K/Akt pathway. *Molecular Therapy - Oncolytics* **2022**, *25*, 1-15, <https://doi.org/10.1016/j.omto.2022.03.004>.
18. Hwang, K.-T.; Kim, Y.A.; Kim, J.; Oh, H.J.; Park, J.H.; Choi, I.S.; Park, J.H.; Oh, S.; Chu, A.; Lee, J.Y.; Hwang, K.R. Prognostic influences of BCL1 and BCL2 expression on disease-free survival in breast cancer. *Scientific Reports* **2021**, *11*, 1-11, <https://doi.org/10.1038/s41598-021-90506-x>.
19. Biondini, M.; Kiepas, A.; El-Houjeiri, L.; Annis, M.G.; Hsu, B.E.; Fortier, A.-M.; Morin, G.; Martina, J.A.; Sirois, I.; Aguilar-Mahecha, A.; Gruosso, T.; McGuirk, S.; Rose, A.A.N.; Tokat, U.M.; Johnson, R.M.; Sahin, O.; Bareke, E.; St-Pierre, J.; Park, M.; Basik, M.; Majewski, J.; Puertollano, R.; Pause, A.; Huang, S.; Keler, T.; Siegel, P.M. HSP90 inhibitors induce GPNMB cell-surface expression by modulating lysosomal positioning and sensitize breast cancer cells to glebatumumab vedotin. *Oncogene* **2022**, *41*, 1701-1717, <https://doi.org/10.1038/s41388-022-02206-z>.
20. Chandra, P.; Sachan, N.; Pal, D. Glycogen Synthase Kinase-3 (GSK-3) Inhibitors as a New Lead for Treating Breast and Ovarian Cancer. *Current Drug Targets* **2021**, *22*, 1548-1554, <https://doi.org/10.2174/1389450122666210203183351>.
21. Wang, N.; Fu, J.; Li, Z.; Jiang, N.; Chen, Y.; Peng, J. The Landscape of PDK1 in Breast Cancer. *Cancers* **2022**, *14*, <https://doi.org/10.3390/cancers14030811>.
22. Năița, A.; Merhi, M.; Inchakalody, V.; Fernandes, Q.; Mestiri, S.; Prabhu, K.S.; Uddin, S.; Dermime, S. The role of PAK4 in the immune system and its potential implication in cancer immunotherapy. *Cellular Immunology* **2021**, *367*, <https://doi.org/10.1016/j.cellimm.2021.104408>.
23. Sureshkumar, B.; Mary, Y.S.; Panicker, C.Y.; Suma, S.; Armaković, S.; Armaković, S.J.; Van Alsenoy, C.; Narayana, B. Quinoline derivatives as possible lead compounds for anti-malarial drugs: Spectroscopic, DFT and MD study. *Arabian Journal of Chemistry* **2020**, *13*, 632-648, <https://doi.org/10.1016/j.arabjc.2017.07.006>.
24. Pinzi, L.; Rastelli, G. Molecular Docking: Shifting Paradigms in Drug Discovery. *International Journal of Molecular Sciences* **2019**, *20*, <https://doi.org/10.3390/ijms20184331>.
25. Frisch, M.J.; Trucks, G.W.; Schlegel, H.B.; Scuseria, G.E.; Robb, M.A.; Cheeseman, J.R.; Scalmani, G.; Barone, V.; Mennucci, B.; Petersson, G.A.; Nakatsuji, H. Gaussian 09, Revision C. 02, Gaussian Inc., Wallingford CT, **2009**.
26. Roy, D.; Todd, K.; John, M. Gauss View; Version 5; Semicem. Inc.: Shawnee Mission, KS, USA, **2009**.
27. Prashanth, J.; Ramesh, G.; Laxman Naik, J.; Kishan Ojha, J.; Venkatram Reddy, B. Molecular geometry, NBO analysis, Hyperpolarizability and HOMO-LUMO energies of 2-azido-1-phenylethanone using Quantum chemical calculations. *Materials Today: Proceedings* **2016**, *3*, 3761-3769, <https://doi.org/10.1016/j.matpr.2016.11.025>.
28. Zhuo, L.-G.; Liao, W.; Yu, Z.-X. A Frontier Molecular Orbital Theory Approach to Understanding the Mayr Equation and to Quantifying Nucleophilicity and Electrophilicity by Using HOMO and LUMO Energies. *Asian Journal of Organic Chemistry* **2012**, *1*, 336-345, <https://doi.org/10.1002/ajoc.201200103>.
29. Thangarasu, S.; Chitradevi, A.; Siva, V.; Shameem, A.; Murugan, A.; Viswanathan, T.M.; Athimoolam, S.; Bahadur, S.A. Structural, Spectroscopic, Cytotoxicity and Molecular Docking Studies of Charge Transfer Salt: 4-Aminiumantipyrine Salicylate. *Polycyclic Aromatic Compounds* **2022**, 1-16, <https://doi.org/10.1080/10406638.2022.2064883>.
30. Koparir, M.; Orek, C.; Koparir, P.; Sarac, K. Synthesis, experimental, theoretical characterization and biological activities of 4-ethyl-5-(2-hydroxyphenyl)-2H-1,2,4-triazole-3(4H)-thione. *Spectrochimica Acta Part A: Molecular and Biomolecular Spectroscopy* **2013**, *105*, 522-531, <https://doi.org/10.1016/j.saa.2012.12.052>.

31. Novena, L.M.; Athimoolam, S.; Anitha, R.; Bahadur, S.A. Synthesis, crystal structure, hirshfeld surface analysis, spectral and quantum chemical studies of pharmaceutical cocrystals of a bronchodilator drug (Theophylline). *Journal of Molecular Structure* **2022**, *1249*, <https://doi.org/10.1016/j.molstruc.2021.13158>.
32. Zochedh, A.; Priya, M.; Shunmuganarayanan, A.; Thandavarayan, K.; Sultan, A.B. Investigation on structural, spectroscopic, DFT, biological activity and molecular docking simulation of essential oil Gamma-Terpinene. *Journal of Molecular Structure* **2022**, *1268*, <https://doi.org/10.1016/j.molstruc.2022.133651>.
33. Ravikumar, C.; Hubert Joe, I. Structural and nonlinear optical properties of cross-conjugated system benzophenone thiosemicarbazone: a vibrational spectroscopic study. *Journal of Raman Spectroscopy* **2011**, *42*, 815-824, <https://doi.org/10.1002/jrs.2788>.
34. Love, R.R. Tamoxifen therapy in primary breast cancer: biology, efficacy, and side effects. *Journal of clinical oncology* **1989**, *7*, 803-815, <http://doi.org/10.1200/JCO.1989.7.6.803>.
35. Sharmili Banu, R.K.; Mohana Priya, I.; Azar Zochedh, S.A. Identification of Novel Bioactive Compounds from Banana Fruit (*Musa sapientum*) as Antidepressant in Pregnant Women: Molecular Docking, Physiochemical and ADMET Evaluation. *Asian Journal of Biotechnology and Genetic Engineering* **2022**.